Eur Biophys J (2006) 35: 459–467
DOI 10.1007/s00249-006-0053-y

ARTICLE

E. Mátyus · L. Monticelli · K. E. Kövér
Z. Xu · K. Blaskó · J. Fidy · D. P. Tieleman

Structural investigation of syringomycin-E using molecular dynamics simulation and NMR

Received: 17 October 2005 / Revised: 16 February 2006 / Accepted: 20 February 2006 / Published online: 17 March 2006

Abstract Syringomycin-E (SR-E) is a cyclic lipodepsinonapeptide produced by certain strains of the bacterium *Pseudomonas syringae pv. syringae*. It shows inhibitory effects against many fungal species, including human pathogens. Its primary biological target is the plasma membrane, where it forms channels comprised of at least six SR-E molecules. The high-resolution structure of SR-E and the structure of the channels are currently not known. In this paper, we investigate in atomic detail the molecular features of SR-E in water by NMR and in water and octane by molecular dynamics simulation (MD). We built a model of the peptide and examined its structure in water and octane in 200 ns MD simulations both with and without distance restraints derived from NMR NOE data. The resulting trajectories show good agreement with the measured NOEs and circular dichroism data from the literature and provide atomistic models of SR-E that are an important step toward a better understanding of the antifungal and antibacterial activity of this peptide.

Electronic supplementary material Supplementary material is available in the online version of this article athttp://dx.doi.org/10.1007/s00249-006-0053-y and is accessible for authorized users.

E. Mátyus (✉) · K. Blaskó · J. Fidy
Institute of Biophysics and Radiation Biology,
Semmelweis University, P.O. Box 263,
1444 Budapest, Hungary
E-mail: szedit@puskin.sote.hu
Tel.: +36-1-2662755
Fax: +36-1-2666656

K. E. Kövér
Department of Inorganic and Analytical Chemistry,
University of Debrecen, Debrecen, Hungary

L. Monticelli · Z. Xu · D. P. Tieleman
Department of Biological Sciences, University of Calgary,
Calgary, Canada

Introduction

Syringomycin-E (SR-E) is a member of a family of cyclic lipodepsinonapeptides produced by certain strains of the bacterium *Pseudomonas syringae pv. Syringae* (Segre et al. 1989). It may play dual roles as a plant virulence factor and an antifungal agent against fungal competitors on the plant surface (Takemoto 1992). SR-E exhibits strong effect against many fungal species, including human pathogens. Its primary biological target is the plasma membrane (Ágner et al. 2000). Although the detailed structure of SR-E is not known, it is thought to adopt amphipathic conformations that facilitate its insertion into lipid bilayers (Kaulin et al. 1998) and the formation of a peptide channel. The channel is formed by six SR-E molecules (Malev et al. 2002), has 12 positive charges and the radius of the aqueous pore is approximately 1 nm (Schagina et al. 1998; Malev et al. 2002). Both the kinetics of channel opening and closing and the channel conductance are strongly voltage dependent and pronouncedly asymmetric (Malev et al. 2001). The SR-E channels are permeable to passive fluxes of mono- and divalent ions across cell plasma membranes (Reidl et al. 1989; Che et al. 1992).

The chemical structure of the SR-E nonapeptide has been elucidated using NMR and mass spectrometry, and the absolute configurations of the chiral Cα atoms have been published (Fukuchi et al. 1990, 1992). SR-E consists of a cyclic nonapeptide head, closed by a lactone formed between the hydroxyl group of an L-Ser side chain and the carboxylate group of 4-Cl-L-Thr, and a hydrophobic 3-hydroxydodecanoic fatty acid tail linked via an amide bond to the L-Ser amino group (Fig. 1).

Pseudomonas syringae pv. syringae produces two other important antifungal agents: the syringotoxin (ST), the structure of which differs from SR-E by five amino acids substitutions in residues 2–6 (Ballio et al. 1990; Dalla Serra et al. 1999), and the more complex syringopeptin-25A (SP-25A), which contains 25 amino

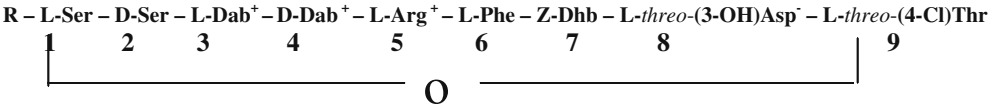

Fig. 1 The chemical structure of SR-E (R = 3-hydroxy-dodecanoic fatty acid; Dab = 2,4-diaminobutanoic acid; Dhb = 2,3-dehydro-2-aminobutiric acid; (3-OH) Asp = 3-hydroxy-aspartic acid; (4-Cl)Thr = 4-chloro-threonine acid)

acids (Ballio et al. 1991). The conformation of SP-25A obtained by computer simulation in vacuo (including NOE data) includes three different structural regions: a loop from residues 2 to 6, a helical region from 8 to 15 and the lactone ring from 18 to 25 (Ballio et al. 1995). The two turns present in the lactone ring of SP-25A are similar to those found in ST investigated by MD (Ballio et al. 1994, 1995).

To understand the effects of SR-E on membranes and to engineer its activity a detailed knowledge of the structure of SR-E is required, but experimental high-resolution methods have not been able to yield structures at atomistic resolution. In this paper, we combine NMR NOE measurements with computer simulations based on available lower resolution structural data to investigate the structure and conformational flexibility of SR-E in water and octane solvent. MD simulations in octane were performed to predict structural preferences of SR-E in a hydrophobic solvent, in particular to investigate the importance of side-chain interactions in determining peptide stability as a first step toward detailed models of the interactions between SR-E and lipid bilayers.

Materials and methods

NMR

The sample was prepared from 4.2 mg of SR-E dissolved in 90% H_2O/10% D_2O at pH 3.7. All NMR spectra were recorded at 311 K on a Bruker Avance DRX-500 spectrometer operating at a ^1H frequency of 500.13 MHz, using a multinuclear proton detected (bbi) single-axis 5-mm gradient probe, processed with the XWINNMR software. Proton chemical shifts were referenced directly to internal 2,2-dimethyl-2-silapentane-5-sulfonate sodium salt (DSS) at 0.00 ppm. A gradient-enhanced, pure absorption phase 2D TOCSY (Kövér et al. 1998) experiment augmented with the Watergate (Sklenár et al. 1993) sequence for solvent suppression was carried out with 62 ms MLEV-17 (Bax and Davis 1985) mixing sequence at an average spin-lock power of 8.33 kHz. The TOCSY spectrum was acquired with 4,096 time domain data points in t_2 and 512 real data points in t_1 with a spectral width of 5,482 Hz in both dimensions. A cosine square window function was applied in both dimensions prior to Fourier transformation. The size of the final matrix was 4,096 (F2) × 1,024 (F1) points.

A combination of water flip-back sequence (Lippens et al. 1995; Grzesiek and Bax 1993; Fulton and Ni 1997), radiation damping suppression using weak bipolar gradient pulses during the t_1 evolution (Sklenár 1995) and an excitation sculpting pulse module (Hwang and Shaka 1995) for further reducing the residual water signal was used for solvent suppression in the NOESY (Kumar et al. 1980) experiment run with a mixing time of 150 ms. The NOESY spectrum was acquired with 2,048 time domain data points in t_2 and 256 complex data points in t_1 with a spectral width of 5,482 Hz in both dimensions. A cosine square window function was applied in both dimensions prior to Fourier transformation. The size of the final matrix was 2,048 (F2) × 1,024 (F1) points. Sequential assignment of proton resonances was obtained using the 2D TOCSY and NOESY spectra proposed by Wüthrich (1986). The NOESY spectrum collected at the mixing time of 150 ms was checked for the absence of spin diffusion effects and then used to infer the intra- and inter-residue dipolar (through space) connectivities. To avoid biasing the structure calculation, only unambiguous NOESY cross-peaks manually assigned were used in the initial structure calculation. Based on the measured volume intensities, the NOESY cross-peaks were classified as strong (*s*), medium (*m*), weak (*w*) and very weak (*vw*) and converted to inter-proton distance estimates (upper limits) of 0.25, 0.35, 0.45 and 0.5 nm, respectively (Wüthrich 1986; Neuhaus and Williamson 1989).

Simulations

An initial model of SR-E was created using the InsightII program (Accelrys) based on the experimental chemical structure and stereo chemistry (Fukuchi et al. 1990, 1992). The SR-E model was solvated in a periodic cubic box of dimensions 3.41×3.41×3.41 nm, large enough to contain the peptide and 0.75 nm of solvent on all sides (1,256 molecules of water, 489 molecules of octane), with either SPC water (Berendsen et al. 1981, 1984) or octane; the total charge on the peptide was +2e, the systems do not contain ions. Because SR-E contains the uncommon amino acid, 2,3-dehydro-aminobutyric acid (Dhb7), and because serine (Ser1) has atoms (involved in the lactone bond) undefined in the ffgmx2 force field used, two molecular fragments X1 and X2 containing the uncommon residues were used to develop parameters (Fig. 2).

Geometry optimizations for X1 and X2 were carried out at the HF level using the 6–31 g basis set. All quantum calculations were performed using the Gaussian 98

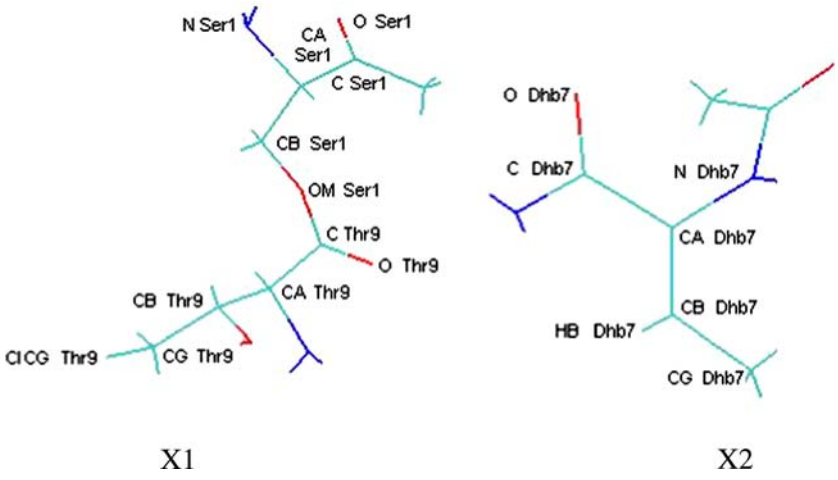

Fig. 2 Structure of the X1 and X2 fragments

programs (Frich et al. 2001). The optimized bond lengths and bond angles from QM results were then used as reference parameters for the missing bond lengths and bond angles in the force filed (Table 1). Force constants for bonds angles were taken from similar groups in the force field. Because bond length was constrained in the production runs their force constants are not critical. For a few atoms we estimated charges by comparison with the charges elsewhere in the force field for consistency.

Each system was energy minimized in 200 steps using the steepest descent algorithm. In all simulations, the temperature was kept at 300 K and the pressure at 1 bar, using the weak coupling method with $\tau_T = 0.1$ ps and $\tau_P = 1$ ps, respectively (Berendsen et al. 1984). In water we carried out two simulations: one without any restraints and one in which the experimentally determined 42 NOEs were incorporated as additional restraints. The GROMACS ffgmx2 force field was used in both cases (Berendsen et al. 1995). This force field has the same parameters as the more commonly used ffgmx force field but has explicit non-polar hydrogen atoms. Although these atoms do not interact with the system, they are used for calculating NOEs and for incorporating distance restraints based on NOEs. Bonds were constrained using LINCS for the peptide and octane (Hess et al. 1997) and the SETTLE algorithm for water (Miyamoto and Kollman 1992). Electrostatics and Lennard–Jones interactions were calculated using a twin-range cut-off of 0.8/1.4 nm. Interactions within the short-range cut-off were updated every time step (2 fs), whereas interactions within the long-range cut-off were updated every ten steps together with the pair list. All atoms were given an initial velocity obtained from a Maxwellian distribution at the desired initial temperature. All the simulations were equilibrated for 50 ps with position restraints on the peptide to allow for the relaxation of the solvent molecules. The equilibrated water-SR-E system was simulated for 200 ns, a length essential to accurately compare the simulations to NOE data (Duan and Kollman 1998; Monticelli and Colombo 2004; Monticelli et al. 2005). In one simulation (resW-SRE) NOE restraints were applied, in the second simulation (W-SRE) no restraints were applied. Distances were restrained by adding a non-physical term to the potential function when the distance between specified pairs of atoms exceeds the experimentally determined distance. The potential form for distance restraints was quadratic below a specified lower bound and between two specified upper bounds and linear beyond the largest bound. The equilibrated octane-SR-E system (O-SRE) was also simulated for 200 ns, without distance restraints since we do not have NOE information in octane. All simulations and the analysis of the resulting trajectories were done with the GROMACS-3.2.1. software package (Lindahl et al. 2001; van der Spoel et al. 2001).

Cluster analyses were carried out using the GROMOS clustering algorithm as described in Daura et al. (1999) with a cut-off of 0.3 nm. A cut-off value of 0.29 nm between hydrogen and acceptor was considered for a hydrogen bond and a cut-off angle of 60° between donor-hydrogen-acceptor. The interproton distances were calculated for each trajectory separately using $\langle r^{-6} \rangle^{-1/6}$ averaging. A cut-off value of 0.4 nm was used to define salt bridge interactions.

Results

Table 2 shows the 42 experimentally determined NOEs of SR-E in H_2O/D_2O solvent together with the corresponding distances calculated from the restrained and unrestrained simulations. Although we measured 42 NOEs, there are insufficient long-range NOEs to calculate a three-dimensional structure directly from the NMR data. Therefore, we turned to our computational model to investigate its structure over long MD simulations while comparing distances calculated from the trajectory to measured NOEs.

The results show that most NOE restraints are satisfied in both simulation in water. Three violations (entries 29, 31, 33 in Table 2) are found in the starting

Table 1 The charge, bonds length and angles value of X1: the molecular fragment containing the Ser1 and Thr9 residues of SR-E; X2: the molecular fragment containing the Dhb7 residue of SR-E (Fig. 2)

Fragments	X1		X2	
Number	Atoms	Charge	Atoms	Charge
c1	OM Ser1	−0.15	CA Dhb7	0.00
c2	–	–	CB Dhb7	0.00
c3	–	–	HB Dhb7	0.00

	Bonds	Values (nm)	Force const	Bonds	Values (nm)	Force const.
b1	CB Ser1-OM Ser1	0.1415	376,560	C Dhb7-CA Dhb7	0.1507	334,720
b2	OM Ser1-C Thr9	0.1342	376,560	CA Dhb7-N Dhb7	0.1410	418,400
b3	C Thr9-O Thr9	0.1180	502,080	CA Dhb7-CB Dhb7	0.1327	418,400
b4	CG Thr9-ClCG Thr9	0.1796	376,560	CB Dhb7-CG Dhb7	0.1499	334,720
b5	–	–	–	CB Dhb7-HB Dhb7	0.1075	292,880

	Angles			Angles		
a1	CA Ser1-CB Ser1-OM Ser1	111.810	460.240	O Dhb7-C Dhb7-CA Dhb7	121.240	502.080
a2	CB ser1- OM Ser1-C Thr9	124.320	502.080	C Dhb7-CA Dhb7-N Dhb7	116.340	502.080
a3	OM Ser1-C Thr9-C Thr9	119.377	418.400	C Dhb7-CA Dhb7-CB Dhb7	121.610	502.080
a4	OM Ser1-C Thr9-CA Thr9	117.897	502.080	N Dhb7-CA Dhb7-CB Dhb7	121.590	502.080
a5	O Thr9-C Thr9-CA Thr9	122.550	502.080	CA Dhb7-N Dhb7-C Phe6	127.950	502.080
a6	CB Thr9-CG Thr9-ClCG Thr9	110.718	520.000	CA Dhb7-CB Dhb7-CG Dhb7	126.170	502.080
a7	–	–	–	CA Dhb7-CB Dhb7-HB Dhb7	117.800	502.080
a8	–	–	–	HB Dhb7-CB Dhb7-CG Dhb7	115.955	502.080

structure. The first and the third one are violated by only 0.01 nm, the second one by 0.11 nm. Averaging the distances over the 200 ns trajectories only one violation is found in both the unrestrained and restrained systems and both of them correspond to medium intensity (entries 31 and 32, respectively, Table 2). These are violated by only 0.01 and 0.02 nm, respectively.

Because of the good agreement between the calculated and measured NOEs, we assume that the long MD simulations provide a reasonable description of the SR-E structure and dynamics. Figure 3 shows the root mean square deviation (RMSD) of the backbone and the whole peptide with respect to the starting structure as function of time for all three simulations (W-SRE, resW-SRE, O-SRE). The backbone RMSD for W-SRE rises initially and levels off at 0.15 nm. The resW-SRE has a similar backbone RMSD curve compared with the W-SRE until ~100 ns, after which the RMSD value fluctuates around 0.24 nm. The SR-E in octane shows a backbone RMSD lower than 0.15 nm for the first ~150 ns of the simulation followed by a transition to an RMSD value of ~0.2 nm. Because about two-thirds of the distance restraints imposed in the resW-SRE simulation involve the amino acid side chains, we expect that the conformational freedom of the side chains would be much more limited in the restrained system. This is confirmed by the difference between the RMSD for all atoms and backbone atoms, which is much larger for W-SRE compared to resW-SRE. SR-E behavior in octane is stable, with the RMSD remaining almost constant at around 0.2 nm. The SR-E remains closer to its starting conformation in the octane than in pure water.

The radius of gyration Rg, a measure of the compactness, of the peptide backbone is ~0.4 nm for both W-SRE and resW-SRE, while it is 0.45 nm for O-SRE (Fig. 4) indicating that the peptide is somewhat less compact in the hydrophobic solvent.

To identify the structures corresponding to the different RMSD levels and to identify the structural differences corresponding to the different radii of gyration in water and octane we used cluster analysis; structures from our 200 ns trajectories were clustered into related conformations based on the whole peptide RMSD. Figure 5 shows the dominant structures for each of the simulations.

Two ensembles of structures characterize the W-SRE trajectory. The **C** and **D** conformers (Fig. 5) are the central structures from the first and second largest clusters, with a population of 81 and 13%, respectively. The **C** conformer has a backbone hydrogen bond between Ser1 and Asp8. The Dhb7 residue is also involved in a hydrogen bond with Ser2. In the second conformer, the hydroxyl group of (3-OH)-Asp8 forms a hydrogen bond with the backbone carbonyl oxygen of Arg5, and a salt bridge is observed between the side chains of the same residues. An important structural difference between the conformers is the location of the phenyl ring and the side chain of Dhb7; both the relative orientation and the distance between the phenyl ring and the Dhb7 side chain change during the simulation, with the distance fluctuating between 0.5 and 0.75 nm. The most significant difference between the two most populated conformers is the position of the alkyl chain, which is elongated in the **D** conformer and folded toward the peptide backbone in the **C** conformer.

Table 2 The experimental and calculated distances of W-SRE and resW-SRE systems, using $\langle r^{-6}\rangle^{-1/6}$ averaging over 200 ns

No	Proton i	Proton j	Experimental distance		Calculated distance of starting structure	Calculated distance of W-SRE	Calculated distance of resW-SRE
1	NH(1)	F(CH_2CO)	0.350	m	0.21	0.24	0.26
2	NH(1)	F(CHCO)	0.550	w	0.55	0.31	0.32
3	NH(1)	Ha(1)	0.550	w	0.30	0.26	0.28
4	NH(1)	Hb(1)	0.550	w	0.36	0.30	0.30
5	NH(2)	Ha(1)	0.350	m	0.21	0.22	0.22
6	NH(2)	Hb(1)	0.550	w	0.33	0.34	0.29
7	NH(2)	Ha(2)	0.550	w	0.26	0.19	0.19
8	NH(2)	Hb(2)	0.550	w	0.42	0.29	0.30
9	NH(2)	Hb′(2)	0.550	w	0.37	0.32	0.31
10	NH(3)	NH(4)	0.600	vw	0.32	0.35	0.35
11	NH(3)	Ha(2)	0.350	m	0.25	0.18	0.19
12	NH(3)	Ha(3)	0.550	w	0.21	0.21	0.23
13	NH(3)	Hb(3)	0.550	w	0.38	0.33	0.35
14	NH(3)	Hg(3)	0.550	w	0.45	0.29	0.30
15	NH(3)	Hg′(3)	0.550	w	0.39	0.26	0.27
16	NH(4)	Hb(4)	0.550	w	0.36	0.32	0.33
17	NH(4)	Hg(4)	0.550	w	0.39	0.34	0.35
18	NH(4)	Hg′(4)	0.550	w	0.29	0.31	0.32
19	NH(5)	NH(4)	0.550	w	0.25	0.37	0.37
20	NH(5)	Hb(5)	0.550	w	0.25	0.24	0.25
21	NH(5)	Hb′(5)	0.350	m	0.24	0.26	0.27
22	NH(5)	Hb(4)	0.550	w	0.37	0.37	0.34
23	NH(5)	Hg(4)	0.550	w	0.53	0.55	0.39
24	NH(5)	Hg′(4)	0.550	w	0.49	0.44	0.48
25	NH(5)	Hg(5)	0.550	w	0.44	0.38	0.36
26	NH(5)	Hg′(5)	0.550	w	0.44	0.34	0.32
27	NH(6)	Ha(6)	0.550	w	0.29	0.27	0.26
28	NH(6)	Ha(5)	0.350	m	0.22	0.22	0.22
29	NH(6)	Hb(6)	0.350	m	0.36	0.23	0.23
30	NH(6)	Hb′(6)	0.350	m	0.25	0.26	0.26
31	NH(6)	Hb(5)	0.350	m	0.46	0.36	0.34
32	NH(6)	Hb′(5)	0.550	w	0.44	0.29	0.57
33	NH(7)	NH(8)	0.350	m	0.36	0.34	0.35
34	NH(7)	Ha(6)	0.350	m	0.27	0.21	0.24
35	NH(7)	Hb(6)	0.550	w	0.20	0.36	0.33
36	NH(7)	Hg(7)	0.550	w	0.28	0.33	0.33
37	NH(8)	Ha(8)	0.550	w	0.29	0.29	0.29
38	NH(8)	Ha(6)	0.550	w	0.37	0.40	0.44
39	NH(8)	Hb(8)	0.600	vw	0.27	0.31	0.20
40	NH(8)	Hg(7)	0.600	vw	0.54	0.49	0.41
41	NH(9)	Hb(8)	0.550	m	0.20	0.20	0.22
42	NH(9)	Hg(9)	0.550	m	0.44	0.29	0.26

Two conformations characterize the resW-SRE system. Figure 5 shows the central structure for the most populated clusters (cluster **E**, 66% of total population, and cluster **F**, 14% of total population). In the **E** conformer, the hydroxyl group of residue Asp8 forms a hydrogen bond with the backbone carbonyl of residue Arg5 and their side chains form a salt bridge, as in the **D** conformer (unrestrained simulation). In the **F** conformer Asp8 is not involved in hydrogen bonding and a salt bridge was not formed. The relative orientation of the phenyl ring of Phe6 and Dhb7 side chain changes during the simulation in a similar way as observed in the W-SRE

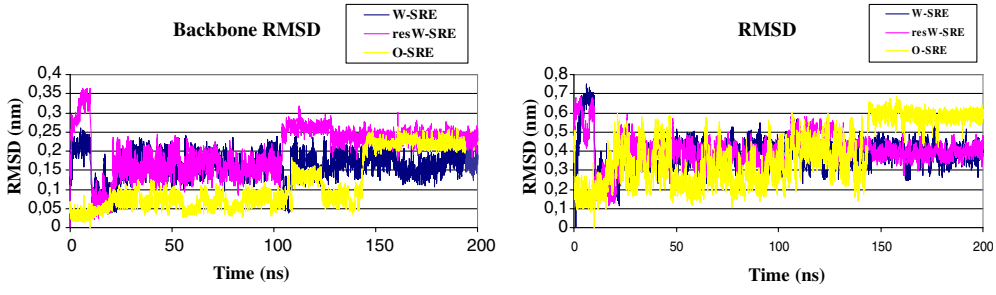

Fig. 3 Backbone and whole peptide root mean square deviation of SRE in a 200 ns MD simulation

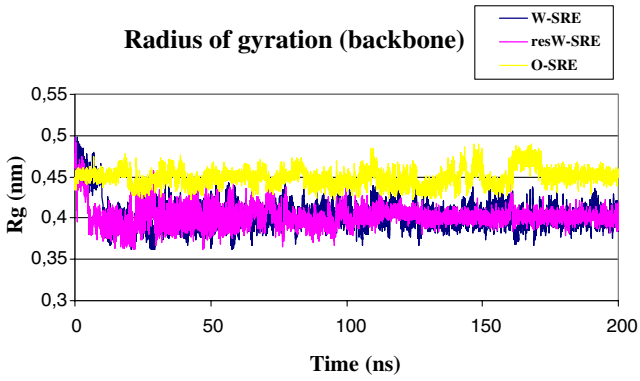

Fig. 4 Radius of gyration of SR-E in a 200 ns MD simulation

simulation: the two side chains, initially far apart and with random orientation (**E** conformer), become closer and assume a parallel orientation (**F** conformer).

In octane, SR-E adopts two dominant conformations with populations of 50 and 30%, respectively (conformer **G** and conformer **H**, Fig. 5). For both clusters, the backbone of the central structure is very similar to the starting structure, with a distorted type II β-turn conformation involving the Phe and Dhb dipeptide as its central residues (Fig. 5, conformation **G**). In both cases the φ, ψ values at the Dhb7 residue differ appreciably from the ideal values for the i + 2 residue, being 40°, 60° in the **G** conformer and 42°, 80° in the **H** conformer, instead of $\varphi = 80°$, $\psi = 0°$ (typical values for the type II β-turn). As a consequence, the distance between the Arg5 amino hydrogen and Asp8 carbonyl oxygen is too long for an intramolecular hydrogen bond in both conformations (0.64 nm and 0.71 nm, respectively). However, the charged side chains of Asp8 and Arg5 form a salt bridge in both conformers. Based on RMSD analysis, a conformational change takes place after ~140 ns because the backbone Rg is constant but the Rg of the whole peptide decreases, the conformational change has to be localized to the side chains. Visual inspection shows that the alkyl chain folds above the plane of the lactone ring (Fig. 5, conformation **H**). This conformation is stabilized by a hydrogen bond between the amino hydrogen of Dab4 and the hydroxyl group of the 3-hydroxydodecanoic acid chain. The radius of gyration Rg for the backbone is higher in octane than in water, indicating that the peptide is less compact in octane. One reason of higher compactness of the backbone in W-SRE should be the stabilization effect of the hydrogen bond between Ser1 and Asp8 which is not detected in O-SRE.

A detailed description of the mobility of the Phe6, Dhb7, Asp8 residues in all three simulations can be obtained by calculating the root mean square fluctuation (RMSF) of the atomic position of the respective residues (Fig. 6).

Asp8 shows the lowest flexibility profile due to the hydrogen bonds involving its hydroxyl oxygen and the

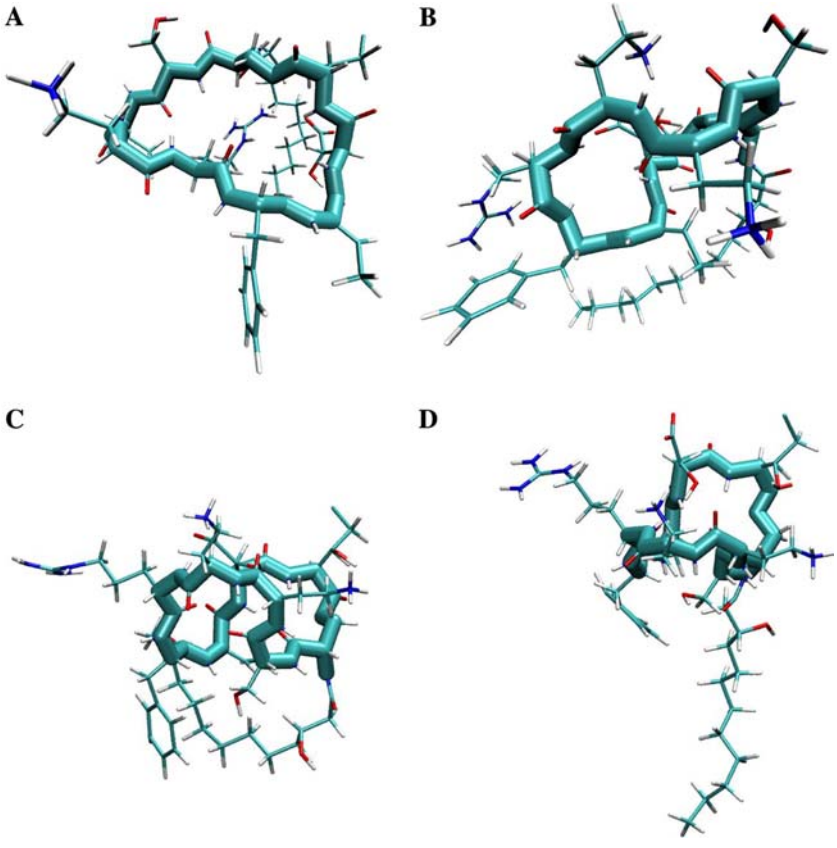

Fig. 5 **A**, **B** The minimized structures of SR-E in water and octane, respectively. **C**, **D** The central structures of SR-E in the W-SRE system. **E**, **F** The central structures of SR-E in the resW-SRE system. **G**, **H** The central structures of SR-E in the O-SRE system

Fig. 5 (Contd.)

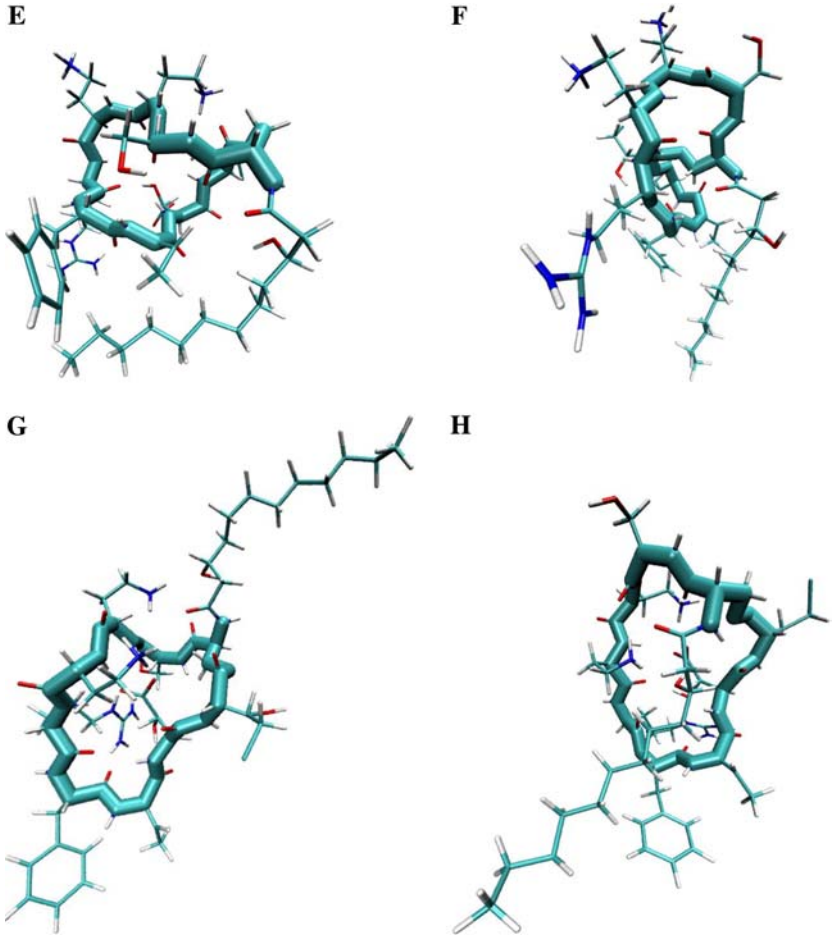

backbone of Ser1 (in the **C** conformer) or Arg5 (in the **D** conformer). A salt bridge was detected between the side chains of Arg5 and Asp8 in both cases. In the resW-SRE simulation, a hydrogen bond between carbonyl oxygen of Arg5 and hydroxyl group of Asp8 is observed in the "open" conformer (Fig. 5**E**), together with a salt bridge between the side chains of the same residues, but these interactions are not found in the "closed" conformer (Fig. 5**F**). In the O-SRE system, the Asp8 residue forms two salt bridges: with Dab3 and Arg5 in the "open" conformer (Fig. 5**G**) and with Dab3 and Dab4 in the "closed" conformer (Fig. 5**H**); it is involved in hydrogen bonds with Dab3 and Arg5 in the "open" conformer and with the hydroxyl group of alkyl chain, but only with Dab4 and Arg5 in the "closed" conformer. The Phe6 and Dhb7 are characterized by higher mobility, with the phenyl ring of Phe6 being the most mobile segment. Its distance from Dhb7 decreased during the simulation and its plane became parallel with the double bond of Dhb7 as shown in Fig. 6.

Discussion

This paper focuses on the investigation at atomic detail of the structural features of SR-E in hydrophobic (octane) and hydrophilic (water) environments as a step toward understanding the membrane activity of SR-E molecule. We measured NMR NOEs for SR-E in water and modeled its structure in solution by molecular dynamics simulations with and without explicit incorporation of the NOE-based distance restrains. The resulting trajectories agree well with the NOE data with

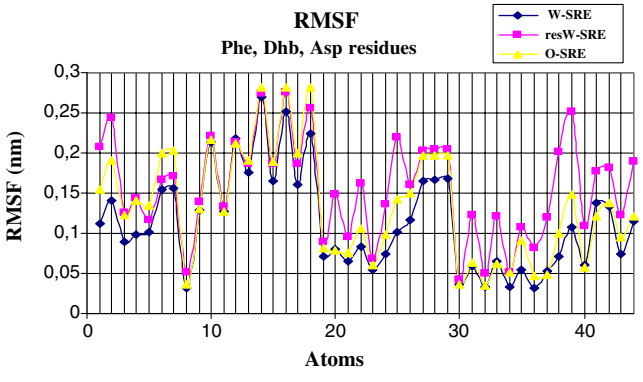

Fig. 6 The RMSF of atoms of the Phe6, Dhb7 and Asp8 residues in a 200 ns MD simulation. The Phe6: backbone 1–4 and 19–20, side chain 5–8, phenil ring 9–18; Dhb7: backbone 21–23 and 30–31, side chain 24–29; Asp8: backbone 32–35 and 43–44, side chain 36–42

only very minor violations. The overall structure of the peptide appears fairly rigid, but becomes somewhat more extended in hydrophobic solvent.

Analyses of the trajectories suggest that two families of structures are sampled in each of the W-SRE, resW-SRE and O-SRE systems. The results of the W-SRE and resW-SRE are very similar, consistent with the fact that both simulations have practically no NOE violations. Both show two dominant structures: a ''closed'' (conformer **C**, **E**) and an ''open'' (conformer **D**, **F**) conformation (Fig. 5) as the dominant structure. In the ''closed'' conformer the alkyl tail is folded across the plane of the lactone ring. Vaillo et al. suggested that the folded tail would also be relatively apolar; therefore the polar groups of the backbone and side chains are involved in hydrogen bonding with one another, and the tail contributes to the overall stability of the SR-E via hydrophobic interaction (Vaillo et al. 1992). Our hydrogen bond analyses, however, reveal that the number of hydrogen bonds in the ''closed'' and ''open'' conformers does not significantly differ.

In the O-SRE system the ''open'' conformer, in which the tail is elongated, (conformer **G**, Fig. 5) has higher population than the ''closed'' one (conformer **H**, Fig. 5), consistent with the expected solubility of the acyl chain in octane. In planar lipid bilayer membranes the tail of SR-E is elongated as well (Kaulin et al. 1998; Bender et al. 1999). The tails of SR-E monomers aggregated into a pore complex reside in the core of the bilayer. The SR-E structure may be similar to O-SRE (conformer **G**).

These simulation results help interpret the results of acetonitrile titration experiments, which clearly revealed the presence of two conformers in an equilibrium that is shifted by changing polarity (Vaillo et al. 1992). One of the two conformers (predominant in aqueous solution) is characterized by a strong interaction between the Dhb7 enone chromophore and the phenylalanyl ring. The possibility of coupling requires that the two groups be in close proximity and that the λmax of the two transitions is similar. Our results reveal that the phenyl ring and Dhb7 side chain are close in space (0.5–0.75 nm) in both the W-SRE and resW-SRE systems. In the hydrophobic environment, the phenyl ring and side chain of Dhb7 residue are more flexible and the distance fluctuates between 1 and 3.5 nm. The likelihood of an interaction between the Dhb7 enone chromophore and the phenilalanyl ring should be lower in an apolar environment than in an aqueous one. This is expected because the strength of this hydrophobic interaction depends on the polarity of the solvent and is higher in water compared to octane.

Experimental studies in model peptides containing dehydrophenylalanine and dehydroleucine show that these residues always favor a type II β-turn conformation, probably as a result of their highly planar nature (Vaillo et al. 1992). Based on the sequence of SR-E such a turn might occur in SR-E, involving the Phe6 and Dhb7 dipeptide as its central residues. This conformation was only observed in the simulations in octane and not in water solvent. Our simulations may provide additional insight into the experimental results: in an apolar solvent the negatively charged Asp8 forms very stable salt bridges with Dab3 and Arg 5, which requires a significant conformational change in the peptide backbone and facilitates the formation of a type II beta turn (Fig. 5, **G** and **H** conformer).

The similarities in primary structure of SR-E and ST suggest a similar conformation. Molecular dynamics simulation (in vacuo) including the 2D NMR NOE data published by Ballio et al. suggests the presence of two turns in the three-dimensional ST lactone ring. Although the primary structure of SP-25A is different from the nonapeptides, the structure of its lactone ring is similar (Ballio 1995). This type of ring structure, resembling the seam of a tennis ball, could not be detected in SR-E conformers. In water, the lactone ring of SR-E has only one turn composed by similar residues (from 5 to 9) as in case of ST. In octane, the shape of the first five residues of the SR-E backbone resembles the first turn of SP-25A lactone ring.

Conclusions

Our results indicate that SR-E exists in two dominant structures whose relative probabilities depend on the polarity of the solvent, in agreement with published experimental data. Using long molecular dynamics simulations we have obtained three-dimensional structures for these two dominant structures that are consistent with NMR NOE measurements. These structures can now be used as a basis to investigate the interactions of SR-E with lipid membranes, the mechanism of channel formation and the structure of channels formed by SR-E.

Acknowledgements This work was supported by Hungarian Scientific Research Fund Grants F 043192, D 048670 and T 048713, by the Natural Science and Engineering Research Council of Canada and by AHFMR postdoctoral fellowships (Luca Monticelli, Zhitao Xu). DPT is an AHFMR Senior Scholar, CIHR New Investigator and Sloan Foundation Fellow. The authors are grateful to Professor Takemoto for providing SR-E for NMR measurements.

References

Ágner G, Kaulin YA, Gurnev PA, Szabó Z, Schagina LV, Takemoto JY, Blaskó K (2000) Membrane-permeabilizing activities of cyclic lipodepsipeptides, syringopeptin 22A and syringomycin E from *Pseudomonas syringae pv. syringae* in human red blood cells and in bilayer lipid membranes. Bioelectrochemistry 52(2):161–167

Ballio A, Bossa F, Collina A, Gallo M, Iacobellis NS, Paci M, Pucci P, Scaloni A, Segre A, Simmaco M (1990) Structure of syringotoxin, a bioactive metabolite of *Pseudomonas syringae pv. syringae*. FEBS Lett 269:377–380

Ballio A, Barra D, Bossa F, Collina A, Grgurina I, Marino G, Moneti G, Paci M, Pucci P, Segre A, Simmaco M (1991) Syringopeptins, new phytotoxic lipodepsipeptides of *Pseudomonas syringae pv. syringae*. FEBS Lett 291:109–112

Ballio A, Collina A, Di Nola A, Manetti C, Pad M, Segre A (1994) Determination of structure and conformation in solution of syringotoxin, a lipodepsipeptide from *Pseudomonas syringae pv. syringae* by 2D NMR and molecular dynamics. Struct Chem 5:43–50

Ballio A, Bossa F, Di Giorgio D, Di Nola A, Manetti C, Paci M, Scaloni A, Segre LA (1995) Solution conformation of the *Pseudomonas syringae pv. syringae* phytotoxic lipodepsipeptide syringopeptin 25-A Two-dimensional NMR, distance geometry and molecular dynamics. Eur J Biochem 234:747–758

Bax A, Davis DG (1985) MLEV-17 based two-dimensional homonuclear magnetization transfer spectroscopy. J Magn Reson 65:355–360

Bender CL, Alarcon-Chaidez F, Gross D (1999) *Pseudomonas syringae* phytotoxins: mode of action, regulation, and biosynthesis by peptide and polyketide syntheses. Microbiol Mol Biol 63:266–292

Berendsen HJC, Postman JPM, van Gunsteren, Hermans J (1981) Intermolecular forces. D. Reidel Publishing Company, Dordrecht, pp 331–342

Berendsen HJC, Postman JPM, van Gunsteren WF, Di Nola A, Haak JRJ (1984) Molecular dynamics with coupling to an external bath. J Chem Phys 81:3684–3690

Berendsen HJC, van der Spoel D, van Drunen R (1995) Gromacs: a message-passing parallel molecular dynamics implementation. Comput Phys Comm 91:43–56

Che FS, Kasamo K, Fukuchi N, Isogai A, Suzuki A (1992) Bacterial phytotoxins, syringomycin, syringostatin and syringotoxin, exert their effect on the plasma membrane H+ -ATPase partly by a detergent action and partly by inhibition of the enzyme. Physiol Plant 86:518–524

Dalla Serra M, Fagiuoli G, Nordera P, Bernhart I, Della Volpe C, Di Giorgio D, Ballio A, Menestrina G (1999) The interaction of lipodepsipeptide toxins from *Pseudomonas syringae pv. syringae* with biological and model membranes: a comparison of syringotoxin, syringomycin, and two syringopeptines. Mol Plant Microbe Interact 12:391–400

Daura X, Gademann K, Jaun B, Seebach D, van Gunsteren WF, Mark AE (1999) Peptide folding: when simulation meets experiment. Angew Chem Int Ed 38:236–240

Duan Y, Kollman PA (1998) Pathways to protein folding intermediate observed in a 1-microdecond simulation in aqueous solution. Science 282:740–744

Frisch MJ, GWT, Schlegel HB, Scuseria GE, Robb MA, Cheeseman JR, Zakrzewski VG, Montgomery JA Jr, Stratmann RE, Burant JC, Dapprich S, Millam JM, Daniels AD, Kudin KN, Strain MC, Farkas O, Tomasi J, Barone V, Cossi M, Cammi R, Mennucci B, Pomelli C, Adamo C, Clifford S, Ochterski J, Petersson GA, Ayala PY, Cui Q, Morokuma K, Salvador P, Dannenberg JJ, Malick DK, Rabuck AD, Raghavachari K, Foresman JB, Cioslowski J, Ortiz JV, Baboul AG, Stefanov BB, Liu G, Liashenko A, Piskorz P, Komaromi I, Gomperts R, Martin RL, Fox DJ, Keith T, Al-Laham MA, Peng CY, Nanayakkara A, Challacombe M, Gill PMW, Johnson B, Chen W, Wong MW, Andres JL, Gonzalez C, Head-Gordon M, Replogle ES, Pople JA. Gaussian Inc., Pittsburgh PA, 2001 (2001). Gaussian 98 Revision A.11

Fukuchi N, Isogai A, Suzuki A (1990) Structure of phytotoxin syringomycin produced by a sugar cane isolate of *Pseudomonas syringae pv. syringae*. Tetrahedron Lett 31:27–31

Fukuchi N, Isogai A, Nakayama J, Takayama S, Yamashita S, Suyama K, Takemoto JY, Suzuki A (1992) Structure and stereochemistry of three phytotoxins syringomycin, syringostatin and syringotoxin produced by *Pseudomonas syringae pv. syringae*. J Chem Perkin Trans 1:1149–1157

Fulton DB, Ni F (1997) ROESY with water flip back for high field NMR of biomolecules. J Magn Reson 129:93–97

Grzesiek S, Bax A (1993) The importance of not saturating H_2O in protein NMR—application to sensitivity enhancement and NOE measurements. J Am Chem Soc 115:12593–12594

Hess B, Bekker H, Berendsen HJ, Fraaije JG (1997) LINCS: a linear constraint solver for molecular simulations. J Comput Chem 18:1463–1472

Hwang TL, Shaka AJ (1995) Water suppression that works: excitation sculpting using arbitrary waveforms and pulse field gradients. J Magn Reson A 112:275–279

Kaulin YA, Schagina LV, Bezrukov SM, Malev VV, Feigin AM, Takemoto JY, Teeter JH (1998) Cluster organization of ion channels formed by the antibiotic syringomycin E in bilayer lipid membranes. Biophys J 74:2918–2925

Kövér KE, Uhrin D, Hruby VJ (1998) Gradient- and sensitivity-enhanced TOCSY experiments. J Magn Reson 130:162–168

Kumar A, Ernst RR, Wüthrich K (1980) Biochem Biophys Res Commun 95:1–6

Lindahl E, Hess B, van der Spoel D (2001) GROMACS 3.0: a package for molecular simulation and trajectory analysis. J Mol Model 7:306–317

Lippens G, Dhalluin C, Wieruszeski JM (1995) Use of water flipback pulse in the homonuclear NOESY experiment. J Biomol NMR 5:327–331

Malev VV, Kaulin YA, Bezrukov SM, Gurnev PA, Takemoto JY, Schagina LY (2001) Kinetics of opening and closure of syringomycin E channels formed in lipid bilayer. Membr Cell Biol 14:813–829

Malev VV, Schagina L, Gurnev P, Takemoto YJ, Nestorovich EM, Bezrukov S (2002) Syringomycin E channel: a lipidic pore stabilized by lipopeptide. Biophys J 82:1985–1994

Miyamoto S, Kollman PA (1992) SETTLE: an analytical version of the SHAKE and RATTLE algorithms for rigid water models. J Comput Chem 13:952–962

Monticelli L, Colombo G (2004) The influence of simulation conditions in molecular dynamics investigations of model β-sheet peptides. Theor Chem Acc 112:145–157

Monticelli L, Tieleman DP, Colombo G (2005) Mechanism of helix nucleation and propagation: microscopic view from microsecond time scale MD simulations. J Phys Chem B 109:20064–20067

Neuhaus D, Williamson MP (1989) The nuclear overhauser effect in structural and conformational analysis, VCH Publ

Reidl HH, Grover TA, Takemoto JY (1989) 31P-NMR evidence for cytoplasmic acidification and phosphate extrusion in syringomycin-treated cells of *Rhodotorula pilimanae*. Biochim Biophys Acta 1010:325–329

Schagina LV, Kaulin YA, Feigin AM, Takemoto JY, Brand JG, Malev VV (1998) Properties of ionic channels formed by the antibiotics syringomycin E in lipid bilayer. Dependence of the electrolyte concentration in the bathing solution. Membr Cell Biol 12:537–555

Segre A, Bachmann RC, Ballio A, Bossa F, Grgurina I, Iacobellis NS, Marino G, Pucci P, Simmaco M, Takemoto JY (1989) The structure of syringomycins A1, E, G. FEBS Lett 255:27–31

Sklenár V (1995) J Magn Reson A 114:132–135

Sklenár V, Piotto M, Leppik R, Saudek V (1993) J Magn Reson A 102:241–245

van der Spoel D, van Drunen R, Berendsen HJC (2001) Groningen machine for chemical simulations. BIOSON Research Institute, Groningen

Takemoto JY (1992) Molecular signals in plant microbe communications. In: Verma DSP (ed) CRC Press, Boca Raton, pp 247–260

Vaillo E, Ballio A, Luisi PL, Thomas RM (1992) The spectroscopic properties of the lipodepsipeptide, syringomycin-E. Biopolymers 32:1317–1326

Wüthrich K (1986) NMR of protein nucleic acids. Wiley-Interscience, New York